Stability of Ni sites across the pressure-induced insulator-to-metal transition in $YNiO_3$

Aline Y. Ramos,[1,*] Cinthia Piamonteze,[2] Hélio C. N. Tolentino,[1] Narcizo M. Souza-Neto,[3] Oana Bunau,[1] Yves Joly,[1] Stéphane Grenier,[1] Jean-Paul Itié,[4] Néstor E. Massa,[5] José A. Alonso,[6] and Maria J. Martinez-Lope[6]

[1]*Institut Néel, CNRS et Université Joseph Fourier, BP 166, F-38042 Grenoble Cedex 9, France*

[2]*Swiss Light Source, Paul Scherrer Institut, CH-5232 Villigen PSI, Switzerland*

[3]*Laboratório Nacional de Luz Síncrotron, P.O. Box 6192, 13084-971 Campinas, São Paulo, Brazil*

[4]*Synchrotron SOLEIL, L'Orme des Merisiers, Saint-Aubin, BP 48, 91192 Gif-sur-Yvette Cedex, France*

[5]*Laboratorio Nacional de Investigación y Servicios en Espectroscopía Óptica-Centro CEQUINOR, Universidad Nacional de La Plata, C.C. 962, 1900 La Plata, Argentina*

[6]*Instituto de Ciencia de Materiales de Madrid, Cantoblanco, E-28049 Madrid, Spain*

(Received 20 September 2011; revised manuscript received 16 December 2011; published 4 January 2012)

The local environment of nickel atoms in $YNiO_3$ across the pressure-induced insulator-to-metal (IM) transition was studied using x-ray absorption spectroscopy (XAS) supported by *ab initio* calculations. The monotonic contraction of the NiO_6 units under applied pressure observed up to 13 GPa stops in a limited pressure domain around 14 GPa, before resuming above 16 GPa. In this narrow pressure range, crystallographic modifications basically occur in the medium to long range, not in the NiO_6 octahedron, whereas the evolution of the near-edge XAS features can be associated with metallization. *Ab initio* calculations show that these features are related to medium-range order, provided that the Ni-O-Ni angle enables a proper overlap of the Ni e_g and O $2p$ orbitals. Metallization is then not directly related to modifications in the average local geometry of the NiO_6 units but more likely to an interoctahedral rearrangement. These outcomes provide evidence of the bandwidth-driven nature of the IM transition.

DOI: 10.1103/PhysRevB.85.045102 PACS number(s): 71.30.+h, 78.70.Dm, 71.15.−m, 71.27.+a

I. INTRODUCTION

The Ni perovskite family $RNiO_3$ (R = Y and Rare Earth except La) presents a localized $3d$-electron behavior at low temperatures and a first-order insulator-to-metal (IM) transition as temperature increases.[1–3] The transition temperature (T_{IM}) is determined by the ionic radius of R that modifies the mismatch between the Ni-O and R-O bond lengths. Such modification goes along with changes in the Ni-O-Ni superexchange angle. A decrease in T_{IM} reflects an increase in the Ni $3d$ e_g and O $2p$ orbital hybridization, concomitant with an increase in the bandwidth.[4] In compounds with small-R ions (Y, Ho, Er, Tm, Yb, and Lu), the crystallographic symmetry changes from monoclinic to orthorhombic across the IM transition.[5–7] The single Ni^{3+} site in the metallic phase splits in the insulating phase into two nonequivalent Ni1 and Ni2 sites, with slightly different average Ni-O distances. These two different average distances are interpreted as a signature of charge order (or charge disproportionation).[5,8,9] It has also been proposed that the difference in Ni local environment reflects the presence of an ionic bonding at Jahn-Teller (JT) distorted Ni2 (larger) sites and covalent bonding at Ni1 (smaller) sites, with possible dynamical fluctuations between both sites.[10,11] Confirming such fluctuations, a strong electron-lattice coupling in a JT-distorted lattice has been evidenced in small-R compounds.[12] For the largest-R compounds the time scale of the fluctuations is expected to be shorter and the splitting is hardly observable by elastic scattering techniques,[9,10] leading to the description of an average structure. Changes in the local symmetry can be tracked by x-ray absorption spectroscopy (XAS).

As a structural technique able to probe dynamical changes, XAS has shown that the two Ni sites coexist in both insulating and metallic states in several $RNiO_3$ compounds.[13,14] In $PrNiO_3$, local symmetry changes accompanying electronic delocalization were found incompatible with the average long-range order proposed from x-ray and neutron diffraction.[15] These studies emphasize the existence of an inhomogeneous structure at the local scale and suggest a common behavior in all $RNiO_3$ compounds for the local electronic and magnetic state.[13]

Among the $RNiO_3$ compounds, $YNiO_3$ presents one of the largest monoclinic distortions at room temperature, due to the small size of the Y^{3+} ions.[6] The thermal-induced metallic phase occurs simultaneously with the vanishing of the long-range monoclinic distortion.[5] However, the coexistence of the two Ni sites, clearly observed by XAS even in the orthorhombic phase,[13,14] supports a model of stable short-range scale distortion.

The application of an external pressure provides a unique tool to further investigate the relationship between structural distortions and electronic properties. Hydrostatic pressure reduces the unit cell volume and shrinks Ni-O bond lengths while straightening the bond angle and stabilizing the metallic phase.[4,16–18] In $YNiO_3$ Garcia Munoz and coworkers reported by x-ray diffraction a sudden structural modification around 14 GPa, consistent with a monoclinic-to-orthorhombic transition.[17] At this pressure, an increase in electronic conductivity and a phonon screening are also observed by infrared spectroscopy. However, the limited resolution of the diffraction experiments did not allow a thorough study of the monoclinic distortion, and the metallic phase was not confirmed.

In the present paper we report *in situ* high-pressure XAS experiments for $YNiO_3$ up to 19 GPa. The expected IM transition is fingerprinted by the XAS near-edge features around 14 GPa. Around that pressure we do not observe any modification in the NiO_6 geometry. The changes mostly come from a rearrangement of the octahedra that leads to

a straightening of the superexchange angle. The subsequent conclusion is that the delocalization of the e_g electrons is due to band effects, enabled in the orthorhombic phase by favorable orbital alignments. Our results show that XAS may provide essential information about octahedral links, hindered in scattering techniques by dynamical fluctuation in the short-range scale. We show that the occurrence of the IM transition is not related to the exact local geometry of the NiO_6 octahedra or charge disproportionation. It essentially depends on the middle-range organization. This confirms the paramount importance of the octahedral tilting in the physics of the nickel perovskites and, in a broader perspective, in correlated electron systems.

II. EXPERIMENT

The pressure-dependent XAS measurements at the Ni K edge (8345 eV) were performed at the dispersive XAS beamline[19,20] of the Laboratório Nacional de Luz Síncrotron, Campinas, Brazil (LNLS). A fine-grained high-quality $YNiO_3$ polycrystalline powder sample[6] was loaded in the 125-μm-diam. hole of an Inconel gasket mounted on 2.4-mm-thick diamond anvils, with a cullet of 300 μm. The spectra were measured using a Si(111) bent crystal monochromator that selected a bandpass of about 800 eV from the white beam and focused it into a Gaussian spot of 150 μm FWHM at the sample position. The gasket cut the tails of the Gaussian beam. However, the beam position for each energy was laterally dispersed in less than 30 μm, such that the full-energy bandpass was transmitted through the gasket with almost the same photon flux. The reference flux, I_0, was measured through a flat piece of glass in order to simulate the average attenuation without introducing new features in the spectra. At each pressure, the cell was realigned at the optical focus. In dispersive XAS there is no mechanical movement of the optics during data collection and the whole spectrum is observed at once. It then is possible to screen the cell orientations in a relatively short time to find an optimal position. The remaining glitches were then removed by small rotations of the cell with respect to the polychromatic x-ray beam. Using a gas-membrane-driven mechanism, the pressure was increased by steps of about 2 GPa, measured using the ruby method.[21] Pressures up to 20 GPa were applied using silicone oil as the pressure medium. Above 15 GPa the nonhydrostatic components of this medium may lead to pressure deviations up to 10% over a diameter of 150 μm. The precision on the pressure is then around 0.5 GPa up to 10 GPa. Above this value, an error bar of 10%, associated with the nonhydrostaticity, is estimated for the absolute pressure scale. Since XAS probes the effective average contribution from all grains randomly oriented over the pressure gradient in the sample area and due to the order of magnitude of the effects (of the order of 10^{-2}), XAS is not very sensitive to a limited nonhydrostaticity.

Extended x-ray-absorption fine structure (EXAFS) data free of Bragg peaks were collected up to about 10.5 $Å^{-1}$. This data range limits the minimum difference between two close distances that can be resolved in the EXAFS analysis to the $\Delta R \simeq 0.15$ Å. In $YNiO_3$ under ambient conditions the average Ni-O distance is 1.994 Å and the separation between the largest and shortest distance is only 0.039 Å.[6] The restricted EXAFS k range ($\simeq$10 $Å^{-1}$) characterizes then a low-resolution study in R space. The Ni-O bond lengths are not distinguishable and bond-length differences within the two Ni sites appear as a static disorder contribution to the total bond-length dispersion.[13] The EXAFS analysis gives only the average distance. The limited k range broadens the Ni-O peak but does not change its average position. Shifts in this average distance with increasing pressure can be tracked precisely, provided that the analysis procedure is strictly the same for the whole series of measurements. The data were analyzed using the ATHENA/ARTEMIS package.[22] The EXAFS oscillations were extracted following the standard procedure of the ATHENA code. The signal corresponding to the oxygen coordination shell was selected by Fourier filtering and the structural parameters were deduced from fitting procedures. In the fitting procedure the number of free parameters was limited by the useful range and the interval corresponding to the selected signal in real space. After a first screening of the individual data sets, all data were fitted together using the option of multiple set analysis. This option increases the number of independent points over the number of free parameters. By setting the same (fitted) origin to the k scale, it reduces substantially the uncertainty of the relative decrease of the Ni-O distances with pressure. The number of neighbors and amplitude factor were fixed. The only amplitude parameter left for each data set is the Debye-Waller term σ, which describes the dispersion of the Ni-O bond lengths. The changes in Ni-O bond length, $\delta R_{\text{Ni-O}}$, and the bond-length dispersion σ are obtained with error bars around 0.005 Å and 0.02 Å, respectively.

For the x-ray absorption near-edge structure (XANES) range the normalization procedure is the same for all pressures. In order to avoid spectra deformation we limit the data handling to simple operations: normalization consists essentially of the subtraction of a straight line for background and to a scaling of the edge jump to 1 in the range 150–250 eV above the edge. Variations in the straight-line subtraction and the exact position of the normalization zone affect to a small extent the overall shape of the spectra but very little the relative intensity of the structures. Owing to the monochromator bandwidth, detector spatial resolution, and the core-hole lifetime, the experimental resolution for the XANES experiments is around 1.5 eV. However, a measure of the shift of the edge energy with pressure is not limited by the experimental resolution but by the stability of the spectrometer and counting statistics. In a dispersive XAS setup the monochromator does not move, allowing a very high energy stability. During the whole experiment, a sharp Bragg peak outside the analysis range allowed us to verify that the energy stability was better than 50 meV, in accordance with previous measurements.[20]

The XANES features were compared to *ab initio* full multiple scattering calculations using the FDMNES code[23] for Ni-centered clusters and with atomic positions given by reported crystallographic structures.[1,6]

III. RESULTS

Figure 1(a) shows the absorption spectrum at ambient pressure and the EXAFS signal for selected pressures (inset). Figure 1(b) gives the Fourier transform modulus (FTM)

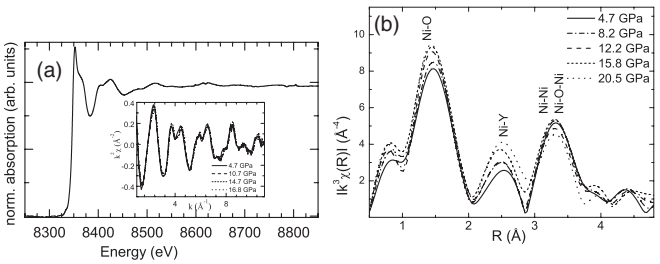

FIG. 1. Absorption spectrum and Fourier transform modulus. (a) Typical Ni K-edge XAS spectrum of $YNiO_3$. Inset: EXAFS signal in the available k range for different pressures. (b) Fourier transform modulus of the EXAFS oscillations for selected pressures.

of these signals. This representation gives the pseudoradial distribution function (not corrected for EXAFS phase shifts) around the average Ni atom. The position of the most prominent peak around 1.5 Å corresponds to the average Ni-O bond length. The next two peaks correspond essentially to the Ni-Y bonds and to the Ni-Ni backscattering and Ni-O-Ni multiple scattering, respectively. These contributions reveal the sensitivity of EXAFS to the next-nearest neighbor's geometry and, so, to the bond angles among octahedra.

The progressive shift of the first peak of the FTM toward shorter distances [Fig. 1(b)] yields the contraction ΔR in the average Ni-O bond lengths. Figure 2 shows the pressure dependence of the Ni-O distance contraction, obtained from the quantitative analysis after selection of that peak. Between 2 and 13 GPa, ΔR decreases almost linearly with the applied pressure. The contraction ΔR up to 13 GPa gives ≈0.033 Å. Such a contraction represents a NiO_6 relative volume decrease of 5.0%. In the same range the unit cell volume measured by diffraction also drops by 5.0%.[17] The monotonic decrease of the Ni-O average distance stops at around 13 GPa. In a transient pressure range ($13 < P < 16$ GPa), the average Ni-O bond length and the distance dispersion remain almost unchanged. Above 16 GPa, the average Ni-O bond length resumes shrinking. The total contraction up to 20 GPa is ≈0.043 Å, or 6.6% in terms of volume decrease. The increase

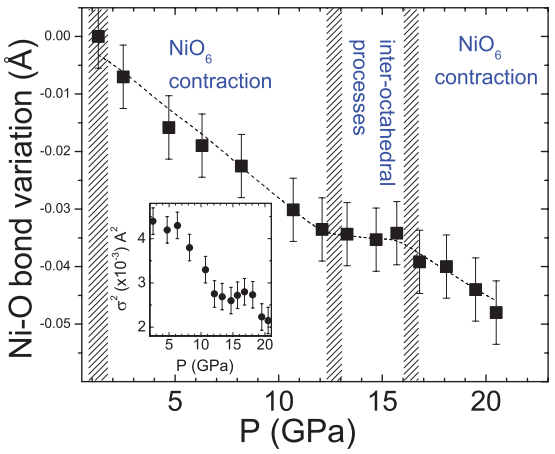

FIG. 2. (Color online) Pressure dependence of the average Ni-O bond-length contraction ΔR obtained from the EXAFS analysis. The line is just a guide for the eyes. Vertical lines separate different regions discussed in the text. Inset: σ^2 as a function of the pressure.

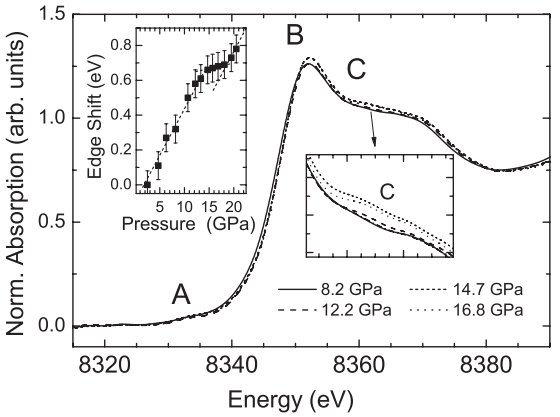

FIG. 3. XANES spectra in $YNiO_3$ for selected representative pressures. A, pre-edge; B, main edge structure; and C, shoulder associated with middle-range effects (see text). Right inset: zoom on the C feature. Left inset: maximum of the derivative at the edge as a function of the pressure.

of the amplitude of the first peak [Fig. 1(b)] corresponds to a decrease in the Ni-O bond-length dispersion. The largest increase occurs from 7 to 13 GPa. Within this range, the average NiO_6 units tend toward a partial symmetrization. The evolution of the Debye-Waller term (Fig. 2, inset) shows that indeed the largest decrease in the bond dispersion occurs from 7 to 13 GPa, confirming this qualitative outcome.

The strongest modifications in the medium-range structures take place within the pressure range 13–16 GPa. As seen in Fig. 1(b), the intensity of the Ni-Y peak increases while that of the Ni-Ni and Ni-O-Ni peaks decreases. These modifications point out interoctahedral rearrangements. Qualitatively, the evolution of position of the Ni-Y peak toward low R is easily interpreted in terms of shortening of the Ni-Y distances. The "shift back" toward larger distances observed at pressures higher than 15 GPa does not fit with such a simple scheme. One may note that already at 15 GPa the peak is substantially enlarged on the high-R side. As this enlargement occurs at the pressure for which the monoclinic-to-orthorhombic transition is expected, it could be a fingerprint of the phase transition and consequently of some interoctahedral rearrangement.

Figure 3 shows the Ni K-edge XANES spectra of $YNiO_3$ at selected pressures. The pre-edge feature A, which probes the Ni $3d$ states hybridized with Ni $4p$ states, does not change within the experimental precision. Two main changes are observed when the applied pressure is increased: a shift of the absorption threshold and subtle modifications of the spectral features B and C.

Edge shifts are primarily associated to changes in the formal valence. However, as here the Ni keeps the form Ni^{3+}, these shifts have essentially a structural origin. As coordination bond lengths decrease, the band energy increases as a result of the higher overlap of the electron density of neighboring atoms. This increased overlap is less significant for localized $1s$ levels than for $4p$ delocalized ones and, consequently, the absorption edge shifts toward higher energies. For small shifts the bond-length reduction (δR) and the associated edge shift (δE) are almost linearly related.[24,25] However, due to the mixture of close Ni-O bonds, such a linear relationship does not strictly

apply in $YNiO_3$, and the evolution of the edge yields only a qualitative analysis.

The edge shift δE is measured by the position of the derivative maximum. The observed shift rate, $\delta E/\delta P$, as a function of applied pressure is not constant over the whole pressure range (Fig. 3, inset). Up to 13 GPa, δE varies linearly with the applied pressure and $\delta E/\delta P$ is about 60 meV/GPa. Within the range $13 < P < 16$ GPa, the edge position shifts at a much slower rate. A new increase in $\delta E/\delta P$ above 16 GPa indicates the recovering of a regime of bond contraction. All these outcomes are in full qualitative agreement with the EXAFS analysis.

Within the range $13 < P < 16$ GPa, a subtle raise of a shoulder C about 10 eV above the main structure B is observed. The emergence of a similar shoulder was reported for $NdNiO_3$ and $PrNiO_3$.[15,26] In these studies it was clearly associated to thermally induced metallization. These authors relate the appearance of the shoulder C to changes in the local atomic environment around Ni at the IM transition. The physical origin of this spectral feature is discussed below. Nevertheless, we can infer that in the present case the shoulder C must also be associated with metallization. We note that its appearance takes place in a narrow range around 14 GPa, where metallization is indeed expected,[17] but also where the EXAFS analysis shows that there is no significant change in the Ni-O bond lengths.

We simulated the Ni K-edge XANES spectra for $YNiO_3$ using *ab initio* full multiple scattering calculations[23] with atomic positions given by crystallographic structures reported by neutron diffraction.[1,6] We observed that the simulations using the monoclinic or the orthorhombic crystallographic structures for $YNiO_3$ lead to identical spectra and do not show the expected C shoulder (Fig. 4). Similar comparison of the calculated spectra in $PrNiO_3$, for the reported orthorhombic structure in the metallic and insulator phases, led Acosta and coworkers[15] to deduce that the changes in the local atomic structure are not reflected in the average crystalline structure. Our results clearly support this view. In addition, the absence of the structure C in our calculation based on the monoclinic structure shows that this feature is not related to the existence of two Ni sites. This suggests that C comes from some characteristics of the local organization beyond the coordination shell.

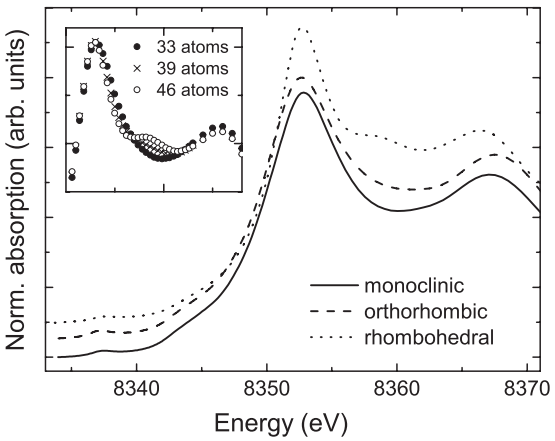

FIG. 4. *Ab initio* simulations of the XANES spectra for a Ni-centered 61-atom cluster of $YNiO_3$ in the monoclinic (solid line), orthorhombic (dashed line), and $LaNiO_3$-like rhombohedral (dotted line) structures. Inset: simulations for the rhombohedral structure and different cluster sizes.

To gather elements about the origin of this feature, we went further by simulating the XANES spectra based on a rhombohedral structure. Even if not reported for $YNiO_3$, the rhombohedral structure corresponds to the most symmetric structure in the $RNiO_3$ series. Importantly, in this structure the tilt angles among adjacent octahedra are quite different compared to those found in monoclinic and orthorhombic $YNiO_3$. This provides a track to interpret our data. The cluster was built from cell parameters deduced from those of $LaNiO_3$ substituting La by Y in the cell. In order to facilitate the comparison with the experimental features in $YNiO_3$, we use an isometric expansion of these parameters, keeping the cell volume to that of $YNiO_3$. In this rhombohedral structure the nickel atoms have a unique regular octahedral site and the superexchange Ni-O-Ni angle is 165°. As for all previous calculations, the cluster contained 61 atoms. The shoulder C is present around 10 eV above B (Fig. 4). We then performed simulations using the same $LaNiO_3$ rhombohedral structure but with decreasing cluster size (Fig. 4, inset). We checked that the C shoulder does not correspond to a specific path of multiple scattering within the octahedron. This structure emerges when the cluster considered in the simulations includes at least 46 atoms (cluster size ≈ 4.8 Å), i.e., half of the neighboring oxygen's octahedra.

IV. DISCUSSION AND CONCLUSION

We used x-ray absorption spectroscopy to describe the evolution of the local and middle-range order under applied pressure. A first regime of monotonic contraction and symmetrization of the average NiO_6 units takes place up to 13 GPa. It stops in a limited pressure domain around 14 GPa, before resuming above 16 GPa. In this narrow pressure range, crystallographic modifications basically occur in the medium to long range, not in the NiO_6 octahedron, whereas the evolution of the near-edge XAS features can be associated with metallization. One important outcome in our experiment is the emergence of the shoulder C in the XANES spectrum around 14 GPa. Such emergence is reproduced in the simulations when the cluster radius reaches a critical value of ≈4.8 Å. It is then not related to the actual very local geometry or symmetrization of the Ni sites but to the middle-range effect. This view is supported by the experimental outcome that the appearance of the shoulder C occurs in a narrow pressure range around 14 GPa where no significant modifications in the average NiO_6 octahedron are observed, whereas significant modifications seem to take place in the middle-range order. We should point out that in the experimental studies reported in $PrNiO_3$ and $NdNiO_3$,[15,26] the shoulder C rising at the IM transition is more intense than in our study. We attributed that to our limited resolution, where a compromise had to be found between good resolution for XANES and the energy range for EXAFS. As a consequence, the absolute intensity of the experimental features of C is not well reproduced in the simulations.

The main effect of pressure is to decrease bond lengths and straighten bond angles, leading to an increased bandwidth

(W) and to a correlated decrease in T_{IM}.[4,27] T_{IM} goes down to room temperature at 14 GPa owing to the increased bandwidth, which changes the ratio W/U, where U is the onsite Coulomb energy. U is not expected to significantly modify around 14 GPa because it concerns much more localized $3d$ orbitals and, in addition, the bond length modification is very small. Although electron-electron correlation (U) represents the main energy in these strong correlated systems, the increase in the bandwidth (W) seems to control the electronic transition.

The presence or absence of the shoulder C around 15 eV above the absorption threshold in the XANES spectra of rare-earth nickelate turns out to be related to the ability of the Ni $3d$ e_g and O $2p$ orbitals to overlap to form a band. In addition to the Ni-O bonding interaction, this ability is strongly related to the Ni-O-Ni angle. The Ni-O-Ni angle crossover for the IM transition at room temperature and pressure in RNiO$_3$ is around 156°.[3,10] In both the monoclinic and orthorhombic crystallographic structures given by neutron diffraction the Ni-O-Ni angle is around 146° in YNiO$_3$, whereas this angle is around 157° in PrNiO$_3$ and NdNiO$_3$. The XANES results are in perfect agreement with the EXAFS outcome that around 14 GPa the reduction of the distance within the octahedra slows down, while a significant reorganization takes place for the Y and Ni next-nearest neighbors. The drop in the lattice parameter c identified by Garcia-Munoz and coworkers at 14 GPa (Ref. 17) corresponds more likely to interoctahedral rearrangements than to a modification in the local geometry of the NiO$_6$ units.

In conclusion, pressure-dependent x-ray absorption spectroscopy in YNiO$_3$ shows that, after an initial shrinking, there are no significant modifications in the average NiO$_6$ octahedra around 14 GPa, where a signature of electronic delocalization is observed. This experimental outcome, supported by *ab initio* XAS calculations, provides evidence of the bandwidth-driven nature of the pressure-induced IM transition in the same way that it has been recently reported for LaMnO$_3$.[28] The electronic delocalization is essentially synchronized with the opening of the Ni-O-Ni angle, and not to a sudden modification in the local geometry of the NiO$_6$ octahedra.

ACKNOWLEDGMENTS

This work is supported by LNLS, CNPq, and CNPq-CNRS agreements. JAA and MJML thank the Spanish MICINN for funding Project No. MAT2010-16404.

*aline.ramos@grenoble.cnrs.fr

[1] J. L. García-Muñoz, J. Rodríguez-Carvajal, P. Lacorre, and J. B. Torrance, Phys. Rev. B **46**, 4414 (1992).
[2] J. B. Torrance, P. Lacorre, A. I. Nazzal, E. J. Ansaldo, and C. Niedermayer, Phys. Rev. B **45**, 8209 (1992).
[3] G. Catalan, Phase Transitions **81**, 729 (2008).
[4] J.-S. Zhou, J. B. Goodenough, B. Dabrowski, P. W. Klamut, and Z. Bukowski, Phys. Rev. B **61**, 4401 (2000).
[5] J. A. Alonso, J. L. García-Muñoz, M. T. Fernández-Díaz, M. A. G. Aranda, M. J. Martínez-Lope, and M. T. Casais, Phys. Rev. Lett. **82**, 3871 (1999).
[6] J. A. Alonso, M. J. Martínez-Lope, M. T. Casais, J. L. García-Muñoz, M. T. Fernández-Díaz, and M. A. G. Aranda, Phys. Rev. B **64**, 094102 (2001).
[7] M. Medarde, C. Dallera, M. Grioni, B. Delley, F. Vernay, J. Mesot, M. Sikora, J. A. Alonso, and M. J. Martínez-Lope, Phys. Rev. B **80**, 245105 (2009).
[8] I. I. Mazin, D. I. Khomskii, R. Lengsdorf, J. A. Alonso, W. G. Marshall, R. M. Ibberson, A. Podlesnyak, M. J. Martínez-Lope, and M. M. Abd-Elmeguid, Phys. Rev. Lett. **98**, 176406 (2007).
[9] U. Staub, G. I. Meijer, F. Fauth, R. Allenspach, J. G. Bednorz, J. Karpinski, S. M. Kazakov, L. Paolasini, and F. d'Acapito, Phys. Rev. Lett. **88**, 126402 (2002).
[10] J.-S. Zhou and J. B. Goodenough, Phys. Rev. B **69**, 153105 (2004).
[11] J.-G. Cheng, J.-S. Zhou, J. B. Goodenough, J. A. Alonso, and M. J. Martinez-Lope, Phys. Rev. B **82**, 085107 (2010).
[12] M. Medarde, P. Lacorre, K. Conder, F. Fauth, and A. Furrer, Phys. Rev. Lett. **80**, 2397 (1998).
[13] C. Piamonteze, H. C. N. Tolentino, A. Y. Ramos, N. E. Massa, J. A. Alonso, M. J. Martínez-Lope, and M. T. Casais, Phys. Rev. B **71**, 012104 (2005).
[14] C. Piamonteze, H. C. N. Tolentino, and A. Y. Ramos, Nucl. Instrum. Methods Phys. Res., Sect. A **246**, 151 (2006).
[15] M. Acosta-Alejandro, J. M. de León, M. Medarde, P. Lacorre, K. Konder, and P. A. Montano, Phys. Rev. B **77**, 085107 (2008).
[16] P. C. Canfield, J. D. Thompson, S.-W. Cheong, and L. W. Rupp, Phys. Rev. B **47**, 12357 (1993).
[17] J. L. García-Muñoz, M. Amboage, M. Hanfland, J. A. Alonso, M. J. Martinez-Lope, and R. Mortimer, Phys. Rev. B **69**, 094106 (2004).
[18] X. Obradors, L. M. Paulius, M. B. Maple, J. B. Torrance, A. I. Nazzal, J. Fontcuberta, and X. Granados, Phys. Rev. B **47**, 12353 (1993).
[19] H. C. N. Tolentino, J. C. Cezar, N. Watanabe, C. Piamonteze, N. M. Souza-Neto, E. Tamura, A. Y. Ramos, and R. Neueschwander, Phys. Scr. **115**, 977 (2005).
[20] J. C. Cezar, N. M. Souza-Neto, C. Piamonteze, E. Tamura, F. Garcia, E. J. Carvalho, R. T. Neueschwander, A. Y. Ramos, H. C. N. Tolentino, A. Caneiro, N. E. Massa, M. J. Martinez-Lope, J. A. Alonso, and J.-P. Itié, J. Synchrotron Radiat. **17**, 93 (2010).
[21] H. Mao, J. Xu, and P. Bell, J. Geophys. Res., Solid Earth Planets **91**, 4673 (1986).
[22] B. Ravel and M. Newville, J. Synchrotron Radiat. **12**, 537 (2005).
[23] Y. Joly, Phys. Rev. B **63**, 125120 (2001).
[24] N. M. Souza-Neto, A. Y. Ramos, H. C. N. Tolentino, E. Favre-Nicolin, and L. Ranno, Phys. Rev. B **70**, 174451 (2004).
[25] A. Y. Ramos, H. C. N. Tolentino, N. M. Souza-Neto, J.-P. Itié, L. Morales, and A. Caneiro, Phys. Rev. B **75**, 052103 (2007).
[26] M. Medarde, A. Fontaine, J. L. García-Muñoz, J. Rodríguez-Carvajal, M. De Santis, M. Sacchi, G. Rossi, and P. Lacorre, Phys. Rev. B **46**, 14975 (1992).
[27] W. Harrison, *The Electronic Structure and Properties of Solids* (Freeman, San Francisco, 1980).
[28] A. Y. Ramos, N. M. Souza-Neto, H. C. N. Tolentino, O. Bunau, Y. Joly, S. Grenier, J.-P. Itié, A.-M. Flank, P. Lagarde, and A. Caneiro, Europhys. Lett. **96**, 36002 (2011).